SI-HCCI Mode Transitions Without Open-Loop Sequence Scheduling: Control Architecture and Experimental Validation

Patrick Gorzelic
Department of Mechanical Engineering,
University of Michigan,
Ann Arbor, MI 48109
e-mail: pgoz@umich.edu

Anna Stefanopoulou
Department of Mechanical Engineering,
University of Michigan,
Ann Arbor, MI 48109
e-mail: annastef@umich.edu

Jeff Sterniak
Robert Bosch LLC,
Farmington Hills, MI 48331
e-mail: jeff.sterniak@us.bosch.com

This paper describes a model-based feedback control method to transition from spark ignition (SI) to homogeneous charge compression ignition (HCCI) combustion in gasoline engines. The purpose of the control structure is to improve robustness and reduce calibration complexity by incorporating feedback of the engine variables into nonlinear model-based calculations that inherently generalize across operating points. This type of structure is sought as an alternative to prior SI-HCCI transition approaches that involve open-loop calibration of input command sequences that must be scheduled by operating condition. The control architecture is designed for cam switching type SI-HCCI mode transition strategies with practical two-stage cam profile hardware, which previously have only been investigated in a purely open-loop framework. Experimental results on a prototype engine show that the control architecture is able to carry out SI-HCCI transitions across the HCCI load range at 2000 rpm engine speed while requiring variation of only one major set point and three minor set points with operating condition. These results suggest a noteworthy improvement in controller generality and ease of calibration relative to previous SI-HCCI transition approaches. [DOI: 10.1115/1.4036232]

1 Introduction

Homogeneous charge compression ignition (HCCI) combustion is a low temperature gasoline combustion mode that offers improved fuel economy over traditional spark ignition (SI) combustion while maintaining low nitrogen oxide emissions [1]. A major concern for the successful integration of HCCI into conventional engines is that its feasible window is limited to a low to mid speed/load subset of the full engine operating range, with SI combustion covering the remainder of the operating conditions. This implies that the combustion mode must be changed between SI and HCCI during online operation. This combustion mode change poses a difficult control problem because of the high degree of difference between SI and HCCI combustion modes, which necessitates changing many engine variables in a short period of time without significant disruption to the engine performance.

Approaches in the literature for SI/HCCI mode transitions have been predominantly based on open-loop scheduling of actuator sequences. Prior studies [2–11] focus solely on open-loop scheduling. While actuator strategies and degrees of success differ among these studies, they tend to agree that significant calibration effort is necessary to determine successful mode transition sequences. The necessity of determining sequences over operating conditions spanning the full HCCI range further complicates the calibration effort and raises the question of robustness in how the sequences will interpolate and potentially extrapolate from tuned operating points. Model-based feedback control can help alleviate these issues in that the control input is determined automatically through model-based calculations in conjunction with online measurements, which eliminates the need for preprogrammed actuator sequences and can respond in real-time to case-by-case disturbances or inaccuracies that may arise in online operation.

Some studies in the literature have explored the use of model-based and/or feedback control in the SI to HCCI (SI-HCCI) direction of SI/HCCI mode transitions. Widd et al. [12] used proportional + integral (PI) and linear quadratic regulator (LQR) control of fuel quantity and exhaust valve timing in the HCCI phase of the SI-HCCI transition. However, the controllers were not activated until 3-4 cycles after entering HCCI, with all other cycles and actuator commands being determined through scheduled sequences. Yang and Zhu [13] employed linear quadratic throttle control for intake pressure tracking during the SI-HCCI transition, and combined PI control with scheduled feedforward sequences tuned through an iterative learning scheme for fuel quantity control. The remainder of the control architecture was given by scheduled open-loop sequences, with the iterative learning fuel commands and time-varying intake pressure reference commands also being determined as offline optimized sequences. Given the difficulty of this control architecture in handling case-by-case variations [14], a sensitivity-based feedforward controller for the fuel command was proposed in Ref. [14] and shown in simulation to improve robustness to disturbances. However, the sensitivity-based controller did not consider the impact of model error in the fuel input calculation, and all other open-loop sequences remained intact. Ravi et al. [15] designed a linear quadratic Gaussian feedback controller with static feedforward control for fuel injection timing in the SI-HCCI mode transition, but again all other components of the control structure were based on open-loop sequences.

It can thus be seen that, though the works [12–15] take significant strides by introducing model-based and/or feedback elements for certain SI-HCCI transition control objectives, the concept of open-loop actuator sequence scheduling remains a critical part of the control structure. A control architecture that addresses all performance objectives through model-based feedback control, so that calibration involves tuning of only set points and gains, may drastically reduce calibration effort as well as better generalize to multiple scenarios. This paper concerns the development and validation of such a SI-HCCI transition controller. Additionally, the controller is developed for a different high-level mode transition

Contributed by the Dynamic Systems Division of ASME for publication in the Journal of Dynamic Systems, Measurement, and Control. Manuscript received September 29, 2015; final manuscript received February 16, 2017; published online June 1, 2017. Assoc. Editor: Junmin Wang.

strategy than those employed in Refs. [12–15] with modified control considerations so that it supplies a model-based method for this strategy, which previously has only been studied from an open-loop standpoint.

The purpose of this paper is to deliver a model-based feedback control method for SI-HCCI transitions with cam switching strategies that requires calibration of only controller set points and gains and generalizes to multiple operating conditions with minimal tuning. The SI-HCCI direction of the mode transition is addressed exclusively here, as the HCCI-SI direction has been found to require additional treatment due to stronger limitations imposed by manifold dynamics [16]. The HCCI-SI manifold dynamics phenomena will be addressed in a separate work. The proposed SI-HCCI control architecture considers tracking of torque, combustion phasing, and air–fuel ratio (AFR) using the actuators of intake throttle, spark timing, fuel injection timing, and fuel injection quantity, while previous studies [12–15] were limited to a subset of these inputs/outputs. The valve timing commands are specified through calibrated set points and are treated as measured time-varying disturbances. While the valve timing control is still based on open-loop calibration, the specification of set points is far simpler and more intuitive than entire input sequences, and enforces fast valve timing adjustments for shorter mode transitions. The term "cam switching strategy" for which the controller is developed refers to a high-level SI-HCCI actuator strategy similar to those in Refs. [5–10], which has the advantage of circumventing the "residual gas fraction gap" [4] or "unstable area" [11] between SI and HCCI combustion. In this paper, the high-level strategy is explained, along with the control architecture which carries out the strategy.

This paper proceeds as follows: First, a high-level description of the SI-HCCI transition strategy is given in order to convey objectives and constraints of the transition and to set the scenario for controller design. The control architectures for the SI and HCCI phases of the transition are given in the following two sections. Experimental SI-HCCI transition results at several operating conditions are then presented, and finally the main aspects of this paper are summarized. Note that additional details of the mode transition strategy and controller development can be found in Ref. [16].

2 Cam Switching Spark Ignition-Homogeneous Charge Compression Ignition Mode Transition Strategy

The goal of the SI-HCCI mode transition is to shift the engine condition from one of stoichiometric air–fuel ratio with low in-cylinder temperature and residual exhaust gas quantity to one of a lean AFR with high in-cylinder temperature and residual quantity. The major actuator changes to accomplish this shift of condition are:

- Switching the cam profiles from higher lift SI settings to lower lift HCCI settings to induce negative valve overlap (NVO), which enables entrapment of a large amount of residual gas.
- Advancing the exhaust valve closing (EVC) timing before top dead center (TDC) to trap a large residual quantity.
- Opening the throttle to compensate for the reduction in air flow caused by the high residual mass.

The timing and transient paths of these actuator changes are the main features defining the mode transition strategy, as the SI/HCCI start/end points can be defined in steady-state experiments. An illustrative set of cam profiles for high lift SI operation with positive valve overlap and HCCI operation with NVO is portrayed in Fig. 1.

Numerous studies have investigated SI-HCCI mode transition strategies [2–11], though they can be divided into two broad categories. In one category, the cam profiles are switched to low lift at the start of the mode transition, prior to entry to HCCI, and then the EVC timing is gradually advanced to its HCCI position while the throttle is gradually opened to compensate. This type of strategy is employed in Refs. [11] and [13–15] and will be referred to as "cam phasing." In the other category, the cam switch is postponed until the valve timings are phased to a condition such that when the exhaust cam switches to low lift, enough residual is trapped to induce auto-ignition on the cycle immediately following. The exhaust cam switch timing thus determines the entry point to HCCI. This type of strategy is employed in Refs. [2–10] and [12] and will be referred to as "cam switching." While the cam switching strategy suffers from increased sensitivity to the cam profile switch timing and throttle opening timing, it allows the unstable area [11] to be avoided. This is expected to have advantages for lower load conditions where the high dilution in the unstable area can significantly threaten SI combustion stability given the low fuel quantity; although it is outside the scope of this paper to perform a definitive comparison. The control methodology in this paper is developed for the cam switching strategy, with an SI/HCCI engine configuration having a two-stage cam mechanism and cam phaser similar to Refs. [6–10], as opposed to more costly fully flexible valve train devices as in Refs. [2–5].

To illustrate the progression of the cam switching SI-HCCI mode transitions considered in this paper, in-cylinder pressure data from a SI-HCCI mode transition experiment are shown in Fig. 2. A key feature that distinguishes the characteristics of the mode transition is the exhaust recompression/gas exchange (GE) event, and so this is pointed out in the figure. The cycles are indexed with reference to the first HCCI cycle, defined as *HCCI 0*. Starting several SI cycles before the switch to HCCI, the combustion can be observed to follow a typical SI profile with a mild and gradual pressure rise and negligible recompression pressure apparent during gas exchange. As the SI phase of the transition proceeds, the recompression pressure increases slightly, caused by the advancing of the EVC timing. The purpose of this advancing is to reach a point in SI such that when the exhaust cam profile is switched from high to low lift, the EVC timing that results is early enough to trap sufficient residual gas to give auto-ignition. The recompression pressure remains mild in SI because the high lift exhaust cam cannot trap a high residual quantity.

On the final SI cycle *SI-1* of Fig. 2, there is a drastic increase in recompression pressure between the start of the cycle and end of the cycle, which is the result of the exhaust cam switching to low lift and suddenly increasing the trapped residual mass. The cam switch mechanism is designed to switch cam profiles during the closed valve portion of the cycle, so that by the exhaust valve opening (EVO) event of cycle *SI-1*, the low-lift cam is engaged. The mechanism is also designed with an offset between the phasing of the high lift and low lift cam sets (see Fig. 1) so that when the cams are switched, the valve timings instantaneously shift by this offset. Following the cam switch to low lift and large recompression peak, the combustion exhibits a much faster and larger pressure rise, signifying auto-ignition and hence HCCI. After cycle *HCCI 0*, the recompression pressure continues to rise on subsequent cycles as the EVC timing advances to its nominal HCCI condition, which is earlier than the HCCI entry point due to the higher exhaust temperature of SI than HCCI.

Qualitative actuator trajectories to produce an SI-HCCI transition like that in Fig. 2 are depicted in Fig. 3. The figure shows the trajectories of the throttle θ_t and EVC timing θ_{evc}, as well as those for the other relevant inputs of spark timing θ_{sp}, start of fuel injection (SOI) timing θ_{soi}, fuel mass m_f, and intake valve opening (IVO) timing θ_{ivo} which characterizes the intake cam phasing. Notice that at the start of the SI phase of the transition, the θ_{ivo} instantaneously jumps, signifying a cam switch to low lift. This switching of the intake cam to low lift prior to the exhaust cam is incorporated into the strategy because it is convenient for calibration in that the two cams do not have to be tuned to switch to low lift simultaneously, and it allows the intake valve timing to be phased to the optimal low lift breathing position prior to entering HCCI. Experiments indicate that for the engine configuration considered here, the intake switch to low lift has minimal influence

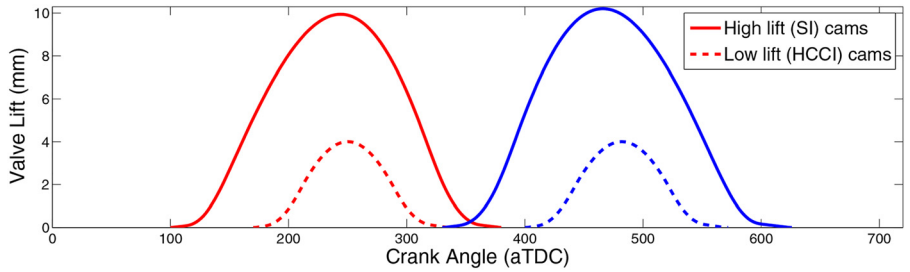

Fig. 1 Illustrative two-stage cam profiles to enable dual SI/HCCI operation

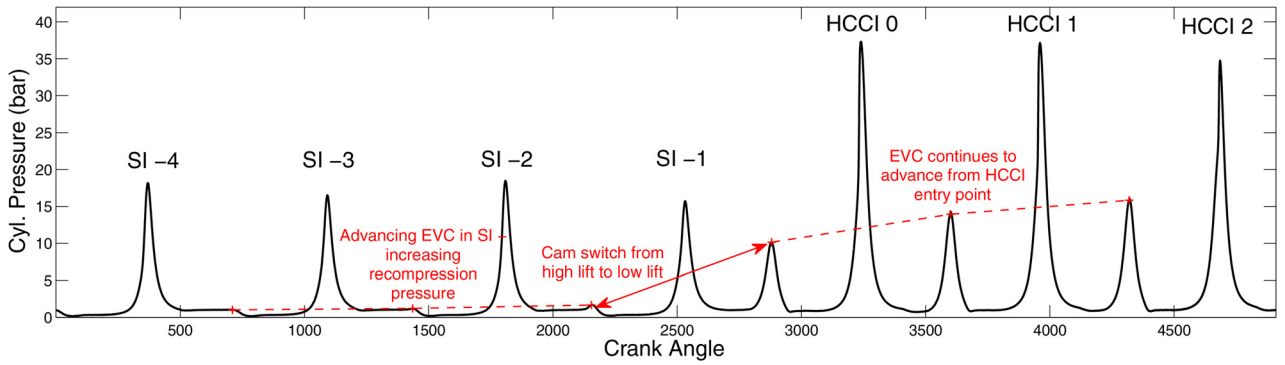

Fig. 2 In-cylinder pressure data from a cam switching SI-HCCI mode transition illustrating the changes in combustion features over the course of the transition

on the air flow dynamics for a significant range of IVO timings, and so is not a major concern for the control strategy. The data indicate that the reduced valve opening height of 4 mm low lift cam height has a minor effect on air flow relative to the timing of the intake breathing events. As long as the low lift IVC timing after the switch is near ($\sim\pm25$ crank angle degrees (CAD)) the optimal volumetric efficiency timing near BDC, the flow is mainly unaffected. For a detailed discussion of these results, please see Ref. [16].

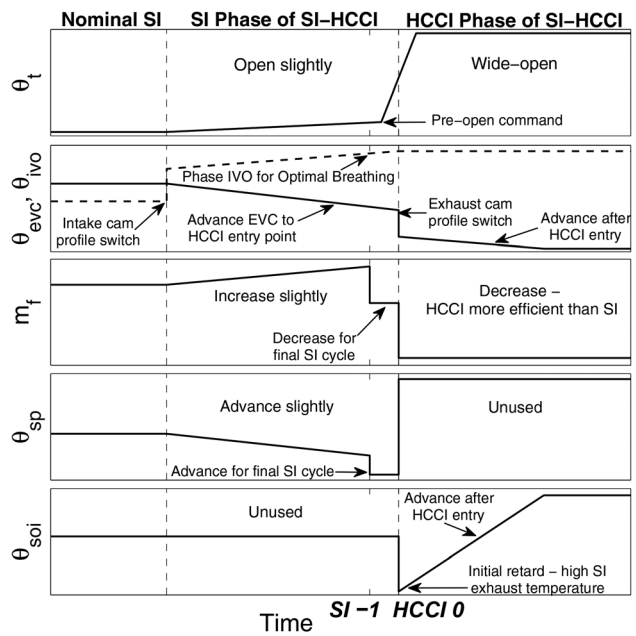

Fig. 3 Representative depiction of high-level actuator trajectories for SI-HCCI transition strategy. θ_{soi} shown with reference to bTDC; all other timings shown with reference to aTDC.

After the intake cam switches to low lift, the SI phase of the mode transition proceeds. The EVC timing is advanced to its switch point for entry to HCCI, while the IVO timing is adjusted to its optimal breathing position for maximum air flow when HCCI is entered. While the valve timings adjust, the throttle compensates for the disturbance to the air flow and engine torque, which usually involves opening past its nominal SI set point. The fuel quantity tends to increase for torque neutrality because the valve timings are phased to nonideal conditions for SI combustion, and so more fuel is necessary to attain the same work output. The spark timing adjusts as necessary to keep the combustion phasing in the desired range, which tends to require spark advance due to the advancing EVC increasing the in-cylinder dilution. The fuel injection timing is unused and left at its nominal SI set point, as it has been observed to have a minor effect on the SI combustion as long as the injection is in the intake stroke.

When the SI-HCCI switching boundary point is reached, a number of notable changes occur. First, the throttle is commanded wide-open to allow for sufficient air flow on the first HCCI cycle. This wide-open command comes slightly in advance of the first HCCI breathing event, to account for the transport delay and manifold/actuator dynamics that require time to overcome and build intake pressure. The fuel may be commanded to reduce on cycle *SI-1*, in order to lean the mixture to reduce the exhaust temperature and combat early combustion phasing on the first HCCI cycle. This reduction in fuel was observed to have minimal impact on the torque for the engine configuration of this paper because it is compensated by an increase in torque on cycle *SI-1* that results from the exhaust cam switch shifting the EVO timing later (see Fig. 1) and elongating the expansion stroke. The spark timing is advanced to compensate for the increased air/residual to fuel ratio caused by the reduction in fuel.

When the exhaust cam switches to low lift, the EVC timing instantaneously jumps by the offset between the high and low lift cam sets, the spark is placed very late so as to not interact with combustion, and the injection timing actuator becomes active as HCCI engages. The injection timing is hypothesized to affect the auto-ignition timing through changing degree of chemical

reactions during recompression [17], with earlier injection giving a longer time for reaction and tending to advance combustion phasing. Hence, SOI is typically late when HCCI is first entered in order to retard the combustion phasing to compensate for the high SI exhaust temperature. As the HCCI phase of the transition carries on, the EVC timing is advanced to trap more residual gas to compensate for the reduction in exhaust temperature from highly dilute HCCI combustion, and the SOI timing advances as well. After several cycles, the exhaust temperature transient settles and the EVC timing reaches its nominal HCCI position, marking the start of nominal HCCI operation.

3 Spark Ignition Phase Controller

3.1 Control Problem Overview. The purpose of the SI phase of the SI-HCCI transition strategy outlined in Sec. 2 is to adjust the valve timings to a point suitable for the switch of the exhaust cam to low lift and entry to HCCI. Throughout this adjustment, there are four main control objectives to consider:

- Deviations of the engine torque from the driver demand should be minimized.
- Deviations of the combustion phasing from max brake torque (MBT) timing should be small enough to avoid deleterious effects on the engine torque and knock/misfire in extreme cases.
- AFR should be kept close to stoichiometric for catalyst efficiency. Any leaning that occurs should be small relative to the catalyst oxygen storage capacity, as filling of the oxygen storage may affect the allowable stay duration in HCCI [18].
- The SI-HCCI switch point should be reached as quickly as possible for fast entry to HCCI.

The controller development addresses these objectives assuming the intake cam has already been switched to low lift, which is the first action of the strategy in Sec. 2.

The model on which the controller is based comes from Ref. [19] and is described in detail in Ref. [16]. This model includes continuous 0D manifold filling dynamics for the air path and discrete cycle to cycle combustion models for SI and HCCI mode. The SI mode combustion model contains no states due to the minor cycle to cycle coupling of SI, while the HCCI combustion model contains three states for cycle to cycle thermal and compositional couplings. Actuator dynamics for the air path valves of throttle and intake/exhaust valve timing were identified from experimental step response data as prototype second-order linear systems, $\ddot{\theta} + 2\zeta\omega_n\dot{\theta} + \omega_n^2\theta = \omega_n^2 u$, where θ represents the valve position and u represents the command input. The model was validated in multiple SI-HCCI transition conditions in Ref. [19].

Given the stated control objectives and the model in Ref. [19], the control problem is formulated according to Table 1. The utilized control inputs are the throttle command, EVC command, IVO command, fuel quantity, and spark timing, which have units of %, aTDC gas exchange, aTDC GE (mg/cycle) and aTDC, respectively. The performance variables of torque, combustion phasing, and AFR are characterized by the net mean effective pressure (NMEP), 50% burn angle θ_{50}, and relative AFR λ. Torque and combustion phasing are treated as reference inputs to be tracked to specified values, targeting the ideal case where the torque follows the driver command perfectly and the combustion phasing stays at the optimal point. The AFR is allowed to fluctuate within some constraints that are chosen in the vicinity of stoichiometry to retain acceptable aftertreatment performance. This policy affords some flexibility for the fuel control to compensate torque disturbances with minimal impact on emissions due to the short duration of the SI phase of the transition. The feedback variables include the intake manifold pressure and temperature p_{im} and T_{im}, as well as the cam phaser positions and engine speed N_{eng}, which are assumed to be measured and treated as disturbances. Values for saturation limits for the actuators are listed; however, all actuators tend to take values near the middle of their saturation range for the SI phase of the transition, and so input constraints are not a serious concern. The states of the model of Ref. [19] in SI mode are reduced to contain only the intake manifold pressure and valve actuator dynamics, where the intake temperature is eliminated with the isothermal assumption (see, e.g., Ref. [20]) and the exhaust manifold pressure is assumed constant at atmospheric for low load operation.

Table 1 Control problem formulation for SI phase of SI-HCCI transition

Control inputs	$u = [u_t\ u_{\text{ivo}}\ u_{\text{evc}}\ m_{\text{f}}\ \theta_{\text{sp}}]^{\text{T}}$
Feedback variables	$y = [p_{\text{im}}\ T_{\text{im}}\ \theta_{\text{ivo}}\ \theta_{\text{evc}}\ N_{\text{eng}}]^{\text{T}}$
Performance variables	$w = [\text{NMEP}\ \theta_{50}\ \lambda]^{\text{T}}$
Reference inputs	$r = [\text{NMEP}^*\ \theta^*_{50,S}]^{\text{T}}$
λ bounds	$\lambda^{\text{rich}} \le \lambda \le \lambda^{\text{lean}}$
Input lower bounds	$u_{\text{low}} = [0\ 10\ -85\ 5\ -60]^{\text{T}}$
Input upper bounds	$u_{\text{high}} = [100\ 110\ 15\ 50\ 50]^{\text{T}}$
Model states	$x = [p_{\text{im}}\ \theta_t\ \dot{\theta}_t\ \theta_{\text{evc}}\ \dot{\theta}_{\text{evc}}\ \theta_{\text{ivo}}\ \dot{\theta}_{\text{ivo}}]^{\text{T}}$

A controller that addressed the SI phase of the SI-HCCI transition with LQR state feedback control was previously proposed in Ref. [21]. The controller development here departs from the structure of Ref. [21], where all actuators were assumed to be operating on the same sampling loop. The controller pursued here is divided into two subsystems for air path control and combustion control so that the air path actuators can operate on a time-synchronous loop and the combustion actuators can operate on a cycle-synchronous loop given their inherent cycle to cycle nature. This architecture is also more convenient for multicylinder engines, where each cylinder has separate combustion outputs and so it becomes ambiguous which cylinder's outputs to use for feedback control of the air path actuators in Ref. [21].

A block diagram of the control architecture for the SI phase of the transition is shown in Fig. 4. In what follows, each subsystem and the elements therein are explained.

3.2 Air Path Control. The overall architecture of the air path control is

- u_{ivo} is stepped to the set point θ^*_{ivo}, which is calibrated for optimal low lift breathing and is stored in a look-up table versus engine speed.
- u_{evc} is stepped to the set point $\theta^{\text{swch}}_{\text{evc}}$, which is calibrated to give a favorable starting point for the HCCI combustion when the exhaust cam is switched to low lift. It is stored in a look-up table versus engine speed and load.
- u_t is commanded through a linear feedback controller $C_t(z)$ to track a time-varying reference intake manifold pressure p^*_{im}.
- The reference p^*_{im} is derived from a model-based calculation to achieve $\text{NMEP} = \text{NMEP}^*$ under the constraints $\lambda = 1$ and $\theta_{50} = \theta^*_{50,S}$ with one step look-ahead valve timing disturbances.

The purpose of the IVO reference θ^*_{ivo} is to adjust the IVO timing to achieve maximum air flow when HCCI is entered, to combat the early combustion phasing that can arise from high in-cylinder temperatures caused by the high SI exhaust temperature. The $\theta^{\text{swch}}_{\text{evc}}$ set point represents a key calibration factor, as it defines the EVC timing on cycle *HCCI 0* through the high lift–low lift cam profile offset (see Fig. 1). The HCCI combustion sensitivity to EVC timing is amplified on the first few HCCI cycles because of the high exhaust temperature giving a greater energy storage per unit trapped residual mass. The motivation for the simple step commands for u_{ivo} and u_{evc} is to phase the valve timings to their desired HCCI entry points as quickly as possible, so as to minimize the time required to reach HCCI. This also results in a simple structure that requires specification of only set points as

opposed to actuator sequences or possibly additional feedback control elements.

The purpose of the intake manifold pressure reference p^*_{im} and throttle tracking controller $C_t(z)$ is to adjust u_t throughout the SI phase to compensate for the disturbance of the valve timing changes to the engine air flow. The reference p^*_{im} is estimated from the SI combustion model such that the resulting air flow is predicted to give NMEP = NMEP* when the stoichiometric amount of fuel is injected ($\lambda = 1$) and θ_{50} is at its reference. Thus, for perfect p^*_{im} tracking, the model predicts that torque can perfectly be maintained with a stoichiometric AFR. To assist the throttle in leading the valve timing disturbances, the θ_{evc} and θ_{ivo} values fed to the p^*_{im} calculation are first propagated one sample time ahead, using the identified second-order actuator dynamic models discretized at the sampling frequency; $\theta^{k+1} = b_1 u^k - (a_1\theta^k + a_0\theta^{k-1})$, where θ^k and θ^{k-1} are the current and previous valve timing measurements, u^k is the valve timing command, and the coefficients a_1, a_0, b_1 come from discretization of the actuator dynamics and are based on ζ, ω_n, and the sample period. p^*_{im} is derived in the Appendix.

The throttle controller $C_t(z)$ is designed as a linear lead filter

$$C_t(z) = k_t \frac{z + n_t}{z + p_t} \tag{1}$$

where k_t, n_t, and $p_t < n_t$ are the gain, zero, and pole, respectively. The linearity of the controller is justified, given that the throttle orifice profile and manifold dynamics are nearly linear in the lower SI load range where it is possible to switch to HCCI. The lead filter structure is chosen in order to follow the high frequency content in the p^*_{im} reference, which changes quickly as the valve timings change. The steady-state error of the controller suffers; however, it is not as important because the SI phase of the transition is quickly terminated when the desired HCCI entry point is reached and so does not dwell at steady-state. The parameters k_t, n_t, p_t are initially tuned based on a linearized and discretized version of the air path model to give good stability margins and response speed; however, they are ultimately tuned in experiment. The set point $\bar{\theta}_t$ is taken equal to the throttle set point in nominal SI operation for simplicity.

It should be noted that stability of the $u_t \to p_{\text{im}}$ loop implies that the eigenvalues associated with states $[p_{\text{im}}, \theta_t, \dot{\theta}_t]$ are stable, and that the eigenvalues for $[\theta_{\text{evc}}, \dot{\theta}_{\text{evc}}, \theta_{\text{ivo}}, \dot{\theta}_{\text{ivo}}]$ are inherently stable because they are actuator dynamics, which are untouched by the controller. Thus, designing $C_t(z)$ for a stable $u_t \to p_{\text{im}}$ loop ensures that all eigenvalues of the system are stable, and thus the full SI phase controller including cross couplings across multiple control loops is stable. It is, however, possible to violate this principle if the $\theta^{\text{swch}}_{\text{evc}}$ set point is chosen very early, which can cause a high amount of residual gas to be trapped and passed between cycles. The combustion may then enter the unstable area noted in Ref. [11], and significant cycle to cycle combustion dynamics may develop for quantities such as temperature and composition whose eigenvalues may or may not be stable. The $\theta^{\text{swch}}_{\text{evc}}$ set point must thus not be placed early enough for these phenomena to occur, which in practice can be gauged by the degree of cyclic variation when $\theta_{\text{evc}} = \theta^{\text{swch}}_{\text{evc}}$.

3.3 Combustion Control. The overall architecture of the combustion control is

- m_f is calculated to give NMEP = NMEP* assuming $\theta_{50} = \theta^*_{50,S}$ through a nonlinear model inversion while maintaining $\lambda \in [\lambda^{\text{rich}}, \lambda^{\text{lean}}]$.
- θ_{sp} is calculated to give $\theta_{50} = \theta^*_{50,S}$ through a nonlinear model inversion.

The idea behind the combustion control structure is to use model inverse-base calculations to cancel any disturbances to the performance outputs that result from valve timing changes and imperfect air path control performance throughout the transition. The model inverse nature of the control laws is advantageous due to the relative degree 0 relationship between the combustion actuators and performance variables, which allows the outputs to be adjusted to their reference without any dynamics for immediate compensation for disturbances. Moreover, the controller need only invert static functions as opposed to system dynamics.

The m_f control input calculation is structured to take into account both torque tracking and AFR constraints. The fuel quantity m^τ_f to attain NMEP = NMEP* with $\theta_{50} = \theta^*_{50,S}$ is first evaluated by inverting the $m_f \to$ NMEP relationship with the measured intake conditions and valve timings, signified by $P_{f-\tau}$ in Fig. 4. The derivation of this expression is given in the Appendix. The AFR that will result with $m_f = m^\tau_f$ is then calculated from the λ expression P_λ

$$\lambda^\tau = \frac{m_a}{m^\tau_f \text{AFR}_s} \tag{2}$$

where m_a is the estimated air mass based on measured intake and valve conditions, and AFR_s is the stoichiometric AFR. Finally, the

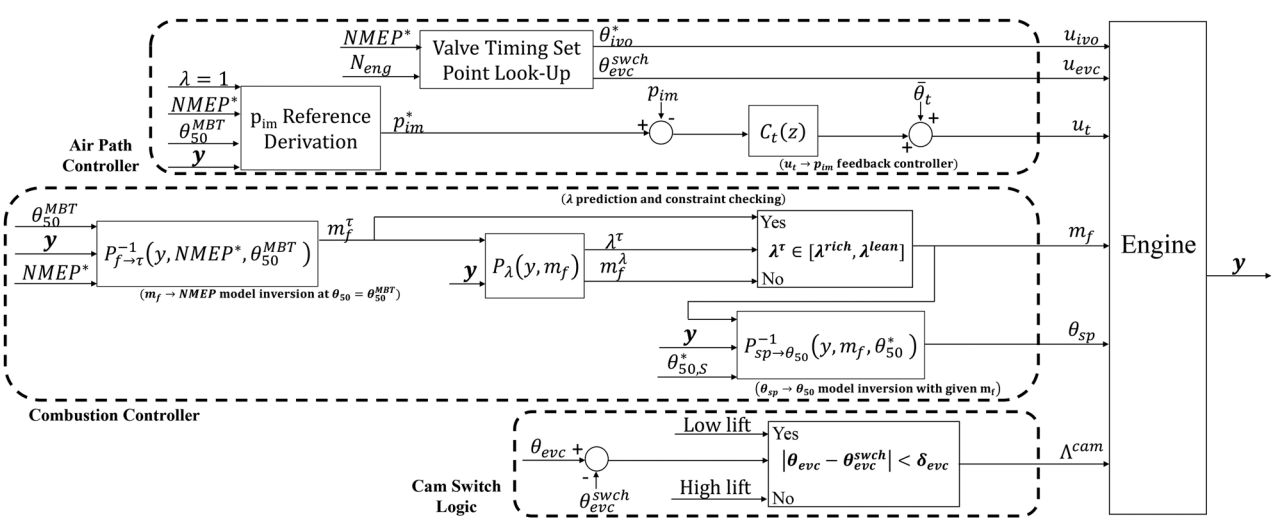

Fig. 4 Block diagram of controller for SI phase of the transition. Variable names are as defined in Table 1. *P* blocks indicate calculations using the plant model, and *C* blocks indicate output feedback controllers.

m_f value is selected from the following logic, in order to enforce AFR constraints

$$m_f = \begin{cases} \dfrac{m_a}{\lambda^{\text{lean}} AFR_s}, & \lambda^{\tau} > \lambda^{\text{lean}} \\ \dfrac{m_a}{\lambda^{\text{rich}} AFR_s}, & \lambda^{\tau} < \lambda^{\text{rich}} \\ m_f^{\tau}, & \text{else} \end{cases} \tag{3}$$

where the relation $m_a/\lambda \text{AFR}_s$ evaluates the fuel quantity necessary to enforce the λ constraints, denoted m_f^{λ} in Fig. 4. The θ_{sp} input comes from a direct inversion of the model's θ_{50} correlation, which is denoted $P_{\text{sp}\to\theta_{50}}$ in Fig. 4. The result is given in the Appendix. Note that the θ_{sp} input is calculated after the m_f input due to the dependence of the θ_{50} correlation on m_f. Also note that the SI combustion model predicts that the combustion control is inherently stable because of its static nature.

While the model inverse-based control laws employed here are advantageous for immediate compensation of disturbances and retaining the accuracy of the full nonlinear model, they still lack a direct means to account for modeling error. Direct output feedback control becomes difficult for the m_f control loop because its output variable can change back and forth between NMEP and λ, and the λ sensor dynamics are long on the timescale of the mode transition. Instead of direct output feedback compensation, an online parameter update scheme will be used to attenuate model error in Ref. [22].

3.4 Cam Switching Logic and the Final Spark Ignition Cycle. The dominant factor responsible for initiating HCCI combustion is the EVC timing, as it determines the trapped residual mass, which is the main thermal actuator for auto-ignition. Hence, the decision to switch the exhaust cam profile Λ^{cam} to low lift and engage HCCI is based on the simple logic that θ_{evc} be within some window δ_{evc} of $\theta_{\text{evc}}^{\text{swch}}$. The tolerance δ_{evc} is tuned to account for the delay in the cam switching mechanism, which for this paper is on the order of 1–2 cycles due to hydraulic system dynamics.

When the decision to switch to HCCI occurs, several other modifications are made. One is to command the throttle to wide-open in advance of the cam switching time, following the actuator strategy depicted in Fig. 3. This is done by setting $\bar{\theta}_t = 100$ when there are $N_{\text{pre}}^{\text{WOT}}$ time steps left before the first low lift breathing event, where $N_{\text{pre}}^{\text{WOT}}$ is a calibration parameter. Additionally, the m_f control bypasses the calculation of m_f^{τ} and chooses m_f solely based on a desired AFR set point λ^{PS}, which enables leaning of the final SI cycle for reduced exhaust temperature and compensation of the torque increase from the shifting EVO. The λ^{PS} value must be balanced with catalyst oxygen fill-up, however.

3.5 Controller Tuning Variables. To summarize the calibration requirements for the SI phase controller, the controller tuning variables are collected in Table 2. The table clearly shows that calibration variables include only a handful of gains and set points, as opposed to entire actuator sequences. Moreover, many of the set points are intuitive to tune and fall in a small feasible range, e.g., $N_{\text{pre}}^{\text{WOT}} \in \{0,1,2,3,4,5\}$, $\lambda^{\text{rich}} \in [.95,1]$, $\lambda^{\text{lean}} \in [1,1.05]$, etc. It is reasonable to assume that the $\theta_{50,S}^*$ and θ_{ivo}^* set points can be taken from the baseline engine calibration, which reduces the number of tuning variables even further.

Table 2 Tuning variables of SI phase controller

Type	Symbol	Description
Gains	k_t, n_t, p_t	Gain, zero, and pole of throttle controller
Set points	$\theta_{\text{evc}}^{\text{swch}}$	θ_{evc} at HCCI switch point
	$N_{\text{pre}}^{\text{WOT}}$	Number of time steps prior to cam switch that throttle is commanded open
	λ^{PS}	λ set point for lean final SI cycle
	$\lambda^{\text{rich}}/\lambda^{\text{lean}}$	Rich/lean λ bounds
	$\theta_{50,S}^*$	θ_{50} set point in SI
	θ_{ivo}^*	θ_{ivo} set point for optimal air flow
	δ_{evc}	θ_{evc} tolerance for switching to HCCI

4 Homogeneous Charge Compression Ignition Phase Controller

4.1 Control Problem Overview. The HCCI phase of the SI-HCCI transition presents the problem of recovering from an unfavorable initial condition to reach a desirable operating point while mitigating disturbances to the performance variables throughout the transient. Once the mode switching transient settles out, the supervisory control may either engage a separate controller or retain the mode transition controller for nominal HCCI operation, depending on the control design. While the HCCI phase proceeds, the controller should target two main objectives:

- Deviations of the engine torque from the driver demand should be minimized.
- Combustion phasing should be kept late enough to minimize pressure rise rate excursions beyond the desired threshold and early enough to avoid combustion instability/misfire.

Note that no AFR objective is specified because it is assumed that the HCCI AFR is always lean, though in general the controller should prevent rich AFRs in HCCI should such conditions arise.

As depicted in Fig. 3, when HCCI is engaged, the throttle is commanded wide-open and the spark timing is placed very late so as not to interact with combustion, eliminating u_t and θ_{sp} from the set of control inputs. Moreover, θ_{ivo} is kept constant at the optimal breathing condition θ_{ivo}^* to which it was commanded in the SI phase of the transition, and so it too requires no control consideration. On the other hand, the SOI timing, which was unused in SI, now becomes an important actuator. Additionally, the combustion model from Ref. [19] now involves states for cycle to cycle couplings, which must be considered in model-based control laws.

Considering the changes to the control objectives, control inputs, and model topology in the HCCI phase of the transition, the control problem is formulated according to Table 3. Torque and combustion phasing are taken as performance variables to be tracked to a specified reference and are again characterized by NMEP and θ_{50}, respectively. The feedback variables now include NMEP and θ_{50}, which are assumed to be available from an in-cylinder pressure measurement. These variables will be used in the HCCI phase for output feedback control and observer-based estimation of the combustion model states of blowdown temperature T_{bd}, burned gas fraction b_{bd}, and fuel mass fraction f_{bd}. The lower saturation limit of θ_{soi} is allowed as late as 180 deg bTDC on cycle *HCCI 0* to compensate for the high residual temperature carried over from SI; on all other cycles, it is limited at 280 deg

Table 3 Control problem formulation for HCCI phase of SI-HCCI transition

Control inputs	$u = [u_{\text{evc}}\ m_f\ \theta_{\text{soi}}]^{\text{T}}$
Feedback	$y = [\text{NMEP}\ \theta_{50}\ p_{\text{im}}\ldots$
Variables	$T_{\text{im}}\ \theta_{\text{ivo}}\ \theta_{\text{evc}}\ N_{\text{eng}}]^{\text{T}}$
Performance variables	$w = [\text{NMEP}\ \ \theta_{50}]^{\text{T}}$
λ rich bound	$\lambda > \lambda_{\min}$
Reference inputs	$r = [\text{NMEP}^*\ \ \theta_{50,H}^*]^{\text{T}}$
Input lower bounds	$u_{\text{low}} = [-120\ \ 5\ \ 180/280]^{\text{T}}$
Input upper bounds	$u_{\text{high}} = [-20\ \ 50\ \ 390]^{\text{T}}$
Model states	$x = [p_{\text{im}}\ \theta_{\text{evc}}\ \dot{\theta}_{\text{evc}}\ T_{\text{bd}}\ b_{\text{bd}}\ f_{\text{bd}}]^{\text{T}}$

bTDC where its authority on θ_{50} tends to diminish in nominal HCCI operation and to allow more time for homogeneous mixing.

A block diagram of the control architecture for the HCCI phase is shown in Fig. 5, where $\hat{x}_c = [\hat{T}_{\text{bd}} \quad \hat{b}_{\text{bd}} \quad \hat{f}_{\text{bd}}]^{\text{T}}$ denotes estimates of the combustion model states. Notice in Fig. 5 that θ_{evc} is governed by a simple step command to a set point as in the SI phase of the transition. The symbol θ^*_{evc} denotes the nominal HCCI θ_{evc} set point for the given speed and load. The logic behind this step command is to quickly advance the EVC timing to its HCCI set point after cycle *HCCI 0*, in order to increase trapped residual mass to compensate for the fast decay of exhaust temperature over the first few HCCI cycles. A prestep factor $N^{\text{EVC}}_{\text{pre}}$ is included to allow the step command to be issued prior to switching to HCCI to give the EVC timing a "head start" in this regard. Given the simplicity of the EVC step command-based control, the remainder of the discussion focuses on the combustion control.

4.2 Combustion Control. The overall architecture of the combustion control is

- m_f tracks NMEP = NMEP* through a nonlinear internal model controller (IMC) assuming $\theta_{50} = \theta^*_{50,H}$. If the required fuel quantity for NMEP = NMEP* causes $\lambda < \lambda_{\text{min}} \approx 1$, the fuel is calculated to fulfill $\lambda = \lambda_{\text{min}}$.
- θ_{soi} tracks $\theta_{50} = \theta^*_{50,H}$ through a nonlinear internal model controller.

Like the SI phase, the combustion control architecture for the HCCI phase is based on relative degree 0 nonlinear model inverse calculations. The main difference is that corrective combustion output feedback for attenuation of model error is incorporated through the IMC structure. Inclusion of combustion output feedback for the HCCI phase is more prudent than for SI, due to the higher sensitivity of the combustion process and more severe transient in the HCCI mode, which makes modeling error a greater concern. Additionally, m_f output feedback control is easier to implement in HCCI than SI since the lower AFR bound λ_{min} is rarely encountered, allowing the NMEP output to be considered exclusively.

The IMC structure by which combustion output feedback is incorporated is depicted in general form in Fig. 6. This structure was chosen because it inherently involves a model inverse calculation and so fits well with the baseline model inverse-based scheme. It additionally offers simple tuning, favorable zero-offset tracking and closed-loop stability properties, and a convenient method to prevent wind-up of the output feedback control in the event of saturated actuators. While the IMC structure provides an inherent plant/model mismatch stability bound of $g((\tilde{P} - P)Q)$

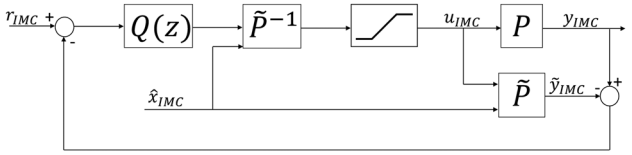

Fig. 6 Diagram of IMC structure. *Q*(*z*) represents a linear low-pass filter, and *P* and $\tilde{P}$ represent the true and controller model of the plant.

where g is the gain operator [23], a linear analysis for a reasonable plant/model mismatch in Ref. [16] shows good stability margins for both m_f and θ_{soi} IMC loops. A technical note is that the low pass filter $Q(z)$ is not strictly necessary for control system causality because of the system's relative degree 0 nature; however, a first-order low pass filter is still included in order to smooth the controller response and reduce sensitivity to noise.

To demonstrate the effect of the IMC feedback, the HCCI phase controller configuration in Fig. 5 is simulated using the HCCI model from Ref. [19] in place of the engine. The internal model controllers follow the form in Fig. 6. In the simulation, an additive model error between the IMC plant model $\tilde{P}$ and the model of Ref. [19] used to represent the engine is injected into the $\theta_{\text{soi}} - \theta_{50}$ loop, and the IMC feedback is allowed to compensate. Noise $\sim N(0, 0.8\,\text{CA}^2)$ is added to the θ_{50} measurement used for feedback, though Fig. 7 shows the θ_{50} response prior to noise addition so that all chattering is due to noise amplification in the feedback loop. The θ_{50} model error is applied for a sufficient duration to allow convergence of θ_{50} to its reference, as well as significant additional time at steady-state where the effect of noise amplification can be clearly observed. As can be seen, when error is injected, the model inverse calculation reacts by driving θ_{50} in the opposite direction. The IMC output feedback corrects for the error over several cycles, at a faster rate but with greater noise amplification as the $Q(z)$ filter pole is made faster. The repeated simulation with doubled error injection in the next subplot below shows that the IMC correction increases in amplitude as modeling error increases. The θ_{50} response follows the same trend, and convergence time is only slightly increased.

The model inverse calculation for the m_f IMC loop is derived from an inversion of the HCCI torque model with respect to fuel using the measured intake conditions and valve timings and estimated combustion states, following a similar procedure to that for m^τ_f in the SI phase controller. Note that to maintain the decentralized m_f/θ_{soi} structure, the assumption that the θ_{soi} controller maintains $\theta_{50} = \theta^*_{50,H}$ is necessary to decouple the torque from the combustion phasing. This is a good assumption for most of the

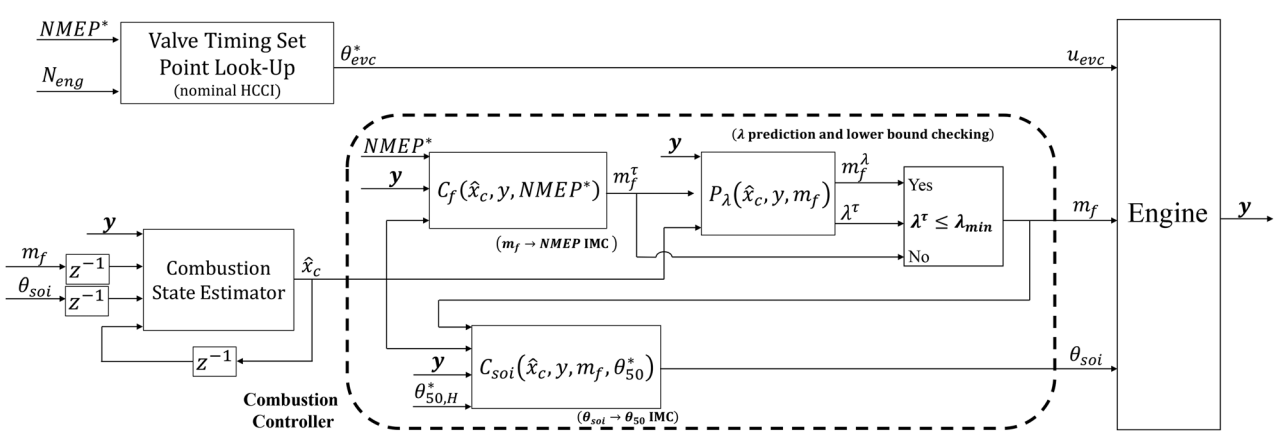

Fig. 5 Block diagram of controller for HCCI phase of the transition. Variable names are as defined in Table 3 with x_c representing combustion states. *P* blocks indicate calculations using the plant model, and *C* blocks indicate output feedback controllers.

HCCI phase of the transition; however, its validity can weaken on cycle *HCCI 0* due to high residual temperature's advancing the combustion phasing beyond the authority of θ_{soi} to compensate. Such early combustion phasing can cause a reduction in torque if the m_f controller assumes $\theta_{50} = \theta^*_{50,H}$. For this reason, the combustion phasing decoupling assumption is modified to $\theta_{50} = \theta^0_{50,f}$ on cycle *HCCI 0*, where $\theta^0_{50,f}$ is tuned to be earlier than $\theta^*_{50,H}$ to alert the fuel control loop to compensate for the effect on the torque. On all other cycles, the decoupling assumption remains unchanged. Note that it was observed in some experimental trials that θ_{50} could be significantly advanced from $\theta^*_{50,H}$ not only on cycle *HCCI 0*, but cycle *HCCI 1* as well. In such cases, the decoupling assumption could be modified with an earlier θ_{50} not only on cycle *HCCI 0* but also on subsequent cycles. This approach was not pursued for the sake of simplicity. The model inverse calculation for the θ_{soi} IMC loop is derived by solving for the θ_{soi} timing to make the Arrhenius threshold of the HCCI combustion model precisely match the integrated Arrhenius rate when $\theta_{50} = \theta^*_{50,H}$. The model inverse calculations for the m_f and θ_{soi} IMC loops are given in the Appendix, along with a method to store the Arrhenius integral in a look-up table for reduced computation time.

4.3 Combustion State Estimator. The dependence of the HCCI combustion control laws given in the Appendix on the HCCI model in-cylinder temperature and composition states T_{bd}, b_{bd}, f_{bd} indicates that these states must be available to carry out the controller calculations. These dependencies arise due to the inherent coupling of the controlled outputs θ_{50} and NMEP to the combustion states in the HCCI model of Ref. [19] used for control. Tracing the output equations for θ_{50} and NMEP in the model of Ref. [19] back to their state dependencies, it can be shown that

$$\theta_{50}(k) \overset{(31)}{=} f(\theta_{soc}(k)) \overset{(27)}{=} f(T_{ivc}(k), \lambda_r(k)) \overset{(4),(11),(12),(18),(22),(24)}{=} f(T_{bd}(k-1), b_{bd}(k-1), f_{bd}(k-1)) \tag{4}$$

$$\text{NMEP}(k) \overset{(48)}{=} f(W_{cig}(k)) \overset{(46)}{=} f(p_{bc}(k), p_{ac}(k), p_{evo}(k)) \overset{(32)-(40)}{=} f(T_{ivc}(k), \theta_{50}(k)) \overset{(4),(11),(12),(18),(24),(27)}{=} f(T_{bd}(k-1), b_{bd}(k-1), f_{bd}(k-1)) \tag{5}$$

where the listed numbers correspond to the equations in Ref. [19] by which the dependencies are introduced. From a high level, these equations show that θ_{50} is influenced by the in-cylinder temperature T_{ivc} and residual AFR λ_r, which are in turn related to the temperature and composition of the exhaust gas from the previous cycle and hence depend on $T_{bd}(k-1), b_{bd}(k-1), f_{bd}(k-1)$. Similarly, NMEP depends on in-cylinder pressure, which is influenced by in-cylinder temperature and combustion phasing, having the same relationships back to the exhaust gas states. For a complete listing of the HCCI model equations, please see Ref. [19] or [16].

Because combustion states represent properties of the in-cylinder gases, they are not directly measurable, and so an observer is included for their estimation. The overall structure of the observer is to use the full nonlinear model in the prediction step of the estimation, while keeping a linear output injection

$$\hat{x}_c(k|k-1) = f(\hat{x}_c(k-1|k-1), u(k-1), y(k-1)) \tag{6}$$

$$\hat{x}_c(k|k) = \hat{x}_c(k|k-1) + L(w(k) - \hat{w}(k|k-1)) \tag{7}$$

where f represents the dynamics of the nonlinear combustion model and L is the observer gain. Note that the combustion performance outputs w are used in the output injection as opposed to the entire output vector y. A block diagram of the observer is shown in Fig. 8.

The idea behind the observer structure is that when first switching to HCCI, little HCCI combustion feedback is accrued until several cycles elapse, starting from *HCCI 0* where there is none at all. Hence, the model predictions are very important, and so the full nonlinear model is employed to carry out the prediction step for improved accuracy relative to a linearized prediction model. The output injection is kept linear mainly for ease of implementation, and is tuned with infinite horizon Kalman filter methodology to balance the tradeoff between process and measurement noise in HCCI combustion. Given the three combustion states and two combustion outputs, the Kalman filter covariance matrices have dimension $W_{est} \in \mathbb{R}^{3\times3}$ for process noise and $V_{est} \in \mathbb{R}^{2\times2}$ for measurement noise. The Kalman gain matrix L is derived by applying the MATLAB function "dlqe" to a linearization of the HCCI model. The linearization operating point is chosen near the center of the HCCI load range so as to extrapolate across low to high load conditions. The gain L is kept constant over all experimental conditions examined in Sec. 5. Note that this simpler nonlinear prediction–linear output injection design was compared with a more sophisticated unscented Kalman filter (UKF) design, which attempts to capture variation of the state to output sensitivities and process/measurement noise covariances due to nonlinearities, which are assumed constant with the linear output injection. It was found in SI-HCCI experiments that the nonlinear prediction–linear output injection and UKF produced similar output injection profiles and overall controller performance. Hence, experiments suggested that there was not much to be gained from the more computationally intensive UKF, and so the simpler design was kept.

The state estimation structure also includes several logical decisions as is apparent from Fig. 8. The first of these logical actions concerns the estimation on cycle *HCCI 0*, where the estimator executes the SI combustion model to generate the prediction step estimates $\hat{x}_c(k|k-1)$ given that the previous combustion is given by SI. Note this is possible without any prior $\hat{x}_c$ estimates due to the static nature of the SI model. Additionally, the output injection is set to 0 because HCCI combustion feedback is not yet available. Another logical action involves switching of the observer gain between a more aggressive value L^0_{est} and a nominally tuned value L_{est} after N^0_{est} HCCI cycles elapse. The motivation for this modification is that, during the first few HCCI cycles, there is a large transient in the combustion dynamics with strong deterministic features. Hence, the deterministic response of the system far outweighs stochastic disturbances from noise, and so measurements can be trusted more closely allowing for a higher observer gain L^0_{est}. In the experiments of this paper, L^0_{est} is generated simply by

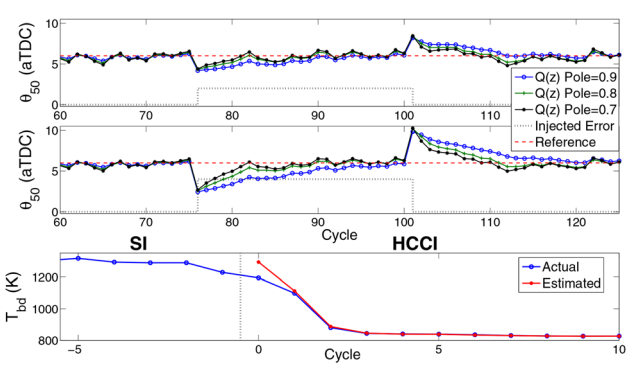

Fig. 7 Top Simulation response of $\theta_{soi}-\theta_{50}$ IMC loop to imposed additive model error for several tunings of the IMC filter $Q(z)$. Middle: Repeated IMC simulation with doubled model error injection. Bottom: True and estimated T_{bd} state values in SI-HCCI mode transition simulation with 100 K initial estimator error.

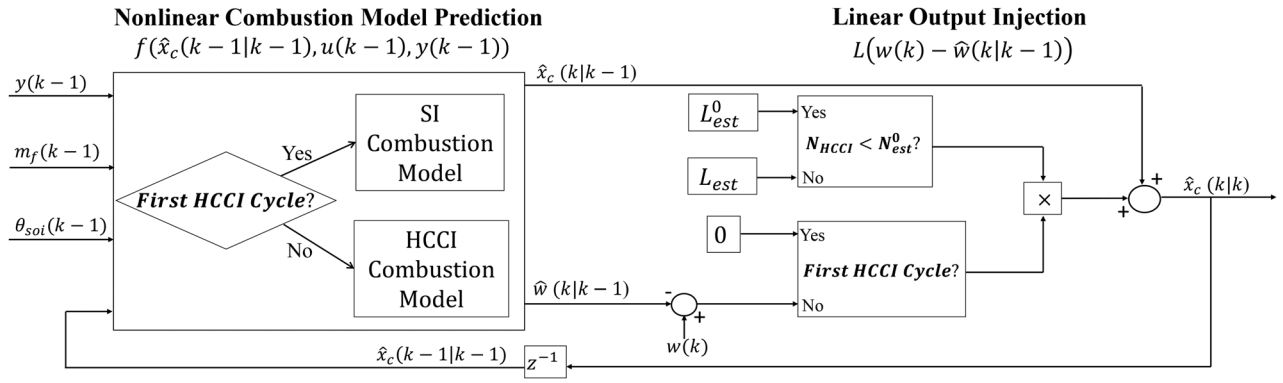

Fig. 8 Diagram of HCCI combustion state estimator

reducing the variance of the θ_{50} measurement in the Kalman filter V_{est} matrix.

A simulation example demonstrating the convergence of the state estimator is given in the bottom subplot of Fig. 7, where the true and estimated T_{bd} state trajectories during a SI-HCCI mode transition are shown. The simulation is again carried out using the configuration of Fig. 5 with the engine replaced by the model of Ref. [19]. The state estimator follows the form in Fig. 8 with the prediction model coming from Ref. [19] but initialized with a state estimation error. As can be seen, the estimated T_{bd} value is initialized with a large (100 K) error from the true value on cycle 0 where HCCI commences. As the T_{bd} value falls off as the system settles to HCCI, the gap between the true and estimated value is rapidly closed, until convergence is obtained after several cycles.

4.4 Controller Tuning Variables. As was done for the SI phase controller, the tuning variables of the HCCI phase controller are collected to convey calibration requirements and displayed in Table 4. As with the SI phase controller, the HCCI phase controller calibration involves tuning a limited number of gains and set points, and again many set points are constrained to a small and intuitive tuning set (e.g., $N^{\text{evc}}_{\text{pre}} \in \{0, 1, 2, 3, 4\}$, $\theta^0_{50,f} \in [-10, 0]$, $\lambda_{\text{min}} \in [1, 1.05]$, etc.). Also, it is reasonable to assume that the nominal HCCI set points θ^*_{evc} and $\theta^*_{50,H}$ come from the baseline engine calibration, in which case these variables need not be included in the HCCI phase controller calibration.

5 Experimental Results

The combined SI-HCCI control architecture described in Secs. 3 and 4 is implemented on an experimental SI/HCCI engine using rapid prototyping software to communicate with the engine control unit. The configuration of the experimental engine is the same as that of the 2 L, four cylinder engine in Ref. [19] with a slightly modified compression ratio of 11.45:1. The engine geometric specifications are provided in Table 5. Feedback of combustion features is supplied through in-cylinder pressure sensors. Each cylinder's exhaust port is equipped with an oxygen sensor for cylinder-individual AFR measurements. The valve system is similar to those in Refs. [6–10] with a two-stage cam mechanism for dual SI/HCCI operation and an electric cam phaser to vary the valve timings. The crank angle offset between the high and low lift cam profiles (see Fig. 1) is characterized by the difference in IVO and EVC timing between the profiles, as the intake and exhaust cam phasing control inputs are specified through these timings. The fuel used in experiments is a 93 Octane, 10% ethanol pump gasoline. Two of the four cylinders displayed unreasonable torque and AFR responses in HCCI mode (e.g., increases in indicated torque accompanied by decreases in AFR for constant fueling), which indicated possible fuel metering errors and/or leakage of lubricant oil into these cylinders. The responses of these two anomalous cylinders are omitted in the following results.

The first experimental SI-HCCI mode transition takes place at an intermediate HCCI load of 2.4 bar NMEP at 2000 rpm and is displayed in Fig. 9. The presented cylinders correspond to the first

Table 5 Experimental engine specifications

Parameter	Value
Displacement	2.0 L
Cylinder arrangement	I4
Compression ratio	11.45
Bore	86 mm
Stroke	86 mm
Con. rod length	145.5 mm
Wrist pin offset	0.8 mm
High/low cam lifts	10 mm/4 mm
High/low cam durations (0.5 mm)	225/114 CAD
IVO high-low cam offset	47 CAD
EVC high-low cam offset	−34 CAD

Table 4 Tuning variables of HCCI phase controller

Type	Symbol	Description
Gains	p_f/p_{soi}	Pole of fuel/SOI IMC filter
	$W_{\text{est}}/V_{\text{est}}$	Kalman filter covariance matrices for combustion state observer
	$W^0_{\text{est}}/V^0_{\text{est}}$	Kalman filter covariance matrices for optional more aggressive observer on first few HCCI cycles
Set	θ^*_{evc}	Nominal HCCI θ_{evc} set point
Points	$N^{\text{evc}}_{\text{pre}}$	Number of time steps prior to cam switch that θ_{evc} is commanded to θ^*_{evc}
	$\theta^*_{50,H}$	θ_{50} set point in HCCI
	$\theta^0_{50,f}$	Assumed θ_{50} in fuel IMC on cycle *HCCI 0*
	λ^{min}	Lower λ bound for lean HCCI

and second of the four to fire on cycle *HCCI 0*, which serves as a limiting case because the intake manifold pressure dynamics have less time to reach atmospheric levels than for the third and fourth cylinders. The first and second cylinders to enter HCCI are referred to as cylinder $H1$ and cylinder $H2$, respectively. Continuous air path input and output responses are interpolated to enable plotting versus cycle along with the discrete combustion input/output responses. As stated in Sec. 3.1, the mode transitions are carried out starting after the intake cam has been switched to low lift at the beginning of the SI phase. This results in a late θ_{ivo} due to the NVO cam design.

The most notable change in the SI phase of the transition in Fig. 9 is the advancing of the EVC timing from its nominal SI set point of 9 deg aTDC to the $\theta_{\text{evc}}^{\text{swch}}$ set point, which is chosen at 23 deg bTDC for this condition. The disturbance caused by the shift of EVC timing causes the throttle to respond first by slightly closing and then slightly opening relative to its nominal position, as the EVC timing passes through inflection point between rebreathing and trapping residual that is around TDC. Throughout this adjustment, the fuel quantity rises to account for the torque disturbance caused by the earlier EVC timing and hence earlier EVO timing reducing the length of the expansion stroke, while respecting the AFR bounds outlined in Sec. 3.1 (here chosen to be [0.97, 1.03]). It can be seen that the NMEP stays close to its reference and the λ deviation from stoichiometry is minimal for both cylinders, which suggests that the throttle and fuel control perform adequately. Note though that the exhaust oxygen sensors have significant low pass filtering characteristics, and so λ deviations may be slightly larger than they appear in Fig. 9. The spark timing control allows some errors in the θ_{50} response, most notably with late θ_{50} for cylinder $H2$ at the beginning and early θ_{50} for cylinder $H1$ toward the end. However, the SI combustion is more robust to perturbations in θ_{50} than is HCCI, and so the effect on the torque response is minimal.

When cycle *HCCI 0* is approached, the throttle is commanded wide-open, giving a rapid rise in intake manifold pressure. The spark is placed very late so as not to interact with combustion, and the EVC timing jumps by the high lift–low lift cam offset (see Fig. 1) as the exhaust cam switches to low lift and HCCI engages. Upon entering HCCI, u_{evc} is stepped to the nominal HCCI set point θ_{evc}^{*} and so θ_{evc} advances. The λ measurements rise lean, with a slower rise in cylinder $H2$ potentially due to differences in oxygen sensor dynamics and transport delay. On cycle *HCCI 0*, the combustion controller places θ_{soi} at the extended lower saturation limit of 180 deg bTDC in anticipation of the high SI exhaust temperature's advancing combustion phasing. However, θ_{50} is still very early on cycle *HCCI 0*, signifying that the exhaust temperature effect is outside the authority of θ_{soi} to compensate, despite that the EVC timing is ≈25 deg later than the nominal HCCI set point. Due to the tuning factor $\theta_{50,f}^{0}$ (here chosen = −6 deg aTDC), the fuel controller anticipates the early θ_{50} and injects a larger quantity so that the torque is minimally affected on cycle *HCCI 0*. However, θ_{50} is again early on cycle *HCCI 1* which the fuel controller does not anticipate, and so a torque reduction results. The SOI controller makes the optimal response to this early θ_{50} for cylinder $H1$ by placing θ_{soi} at its nominal late saturation limit of 280 deg bTDC, though for cylinder $H2$ the controller advances θ_{soi} past the saturation limit. Cylinder $H2$ θ_{50} is more advanced than that of $H1$ over the next few HCCI cycles as well. Further inspection of the controller response data suggests that the more advanced θ_{soi} timing for cylinder $H2$ than $H1$ over the first few HCCI cycles is primarily due to a difference in cylinder air mass and temperature estimation on cycle *HCCI 0*, which carries over to the next few HCCI cycles due to the model's temperature and composition states. This difference is caused by cylinder $H1$'s being predicted to have a lower air mass and hence higher temperature on cycle *HCCI 0* because it occurs earlier in the cycle when the intake pressure has not risen as much. The controller thus predicts an earlier θ_{50} for cylinder $H1$ than $H2$, resulting in a later θ_{soi} timing for $H1$. Other effects that may cause the θ_{50} of cylinder $H2$ to retard more slowly than that of $H1$ include potentially higher estimation error for $H2$ and cylinder to cylinder variability, because a single set of control model parameters is used for all cylinders and cylinder $H2$ is observed to be more prone to knock than $H1$.

Despite some imperfections in the combustion controller, the NMEP stays close to its reference value throughout the transition, with a peak deviation ≈8% for only one cycle. Peak pressure rise rates $dp/d\theta_{\text{max}}$ are higher on the first few HCCI cycles due to earlier combustion phasing, though they remain within the preferred steady-state limit of 6 bar/deg, and so are more than acceptable for the short HCCI transient period. The mode transition is thus largely successful.

To demonstrate the ability of the controller to generalize to multiple conditions, it is exercised to carry out SI-HCCI mode transitions near the engine's low load (≈1.8 bar NMEP) and high load (≈3.2 bar NMEP) HCCI limits at 2000 rpm. This load range is somewhat smaller than those typically reported in the HCCI literature (∼2–4 bar NMEP at 2000 rpm) due to a high cylinder to cylinder variability on the experimental engine. However, the experiments still encompass the range of physical phenomena observed between low and high load HCCI, such as high cyclic variability and ringing, and demonstrate the controller's performance over this range. In the high load case, cylinder $H2$ began

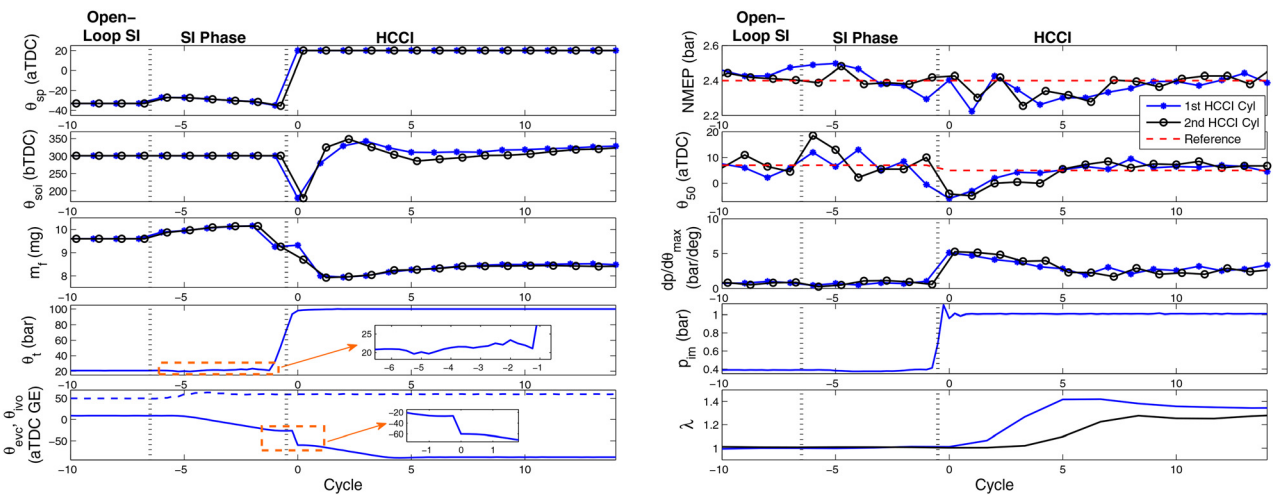

Fig. 9 Controlled SI-HCCI transition at midload HCCI at 2000 rpm. Inputs shown in left column and outputs shown in right column. The first and second cylinders to enter HCCI are referred to as *H*1 and *H*2, respectively.

experiencing problems with runaway knocking and unreasonable AFR/torque responses in HCCI, which are hypothesized to be influenced by carbon deposit build-up based on borescope investigations. To mitigate these effects, a reduced fuel quantity was imposed on cylinder $H2$ at the high load condition, and so its response is omitted in this case.

Summary experimental results for the low load (left) and high load (right) SI-HCCI transition conditions are presented in Fig. 10, where the top three subplots show the combustion inputs and bottom three subplots show the combustion outputs. The θ_{sp} axis is enlarged to show more detail, omitting the late placement of θ_{sp} in HCCI. The plots show that several main features of the actuator trajectories remain common through each condition, with the spark timing advancing and fuel increasing throughout the SI phase, and the SOI timing retarding at the start of the HCCI phase and eventually advancing. However, the actual input command values vary significantly from case to case, which the controller is able to deduce automatically through model-based calculations. The θ_{50} follows a similar response in all cases, starting early in HCCI and retarding to the reference in a few cycles. In the high load case, the early initial HCCI cycles cause $dp/d\theta_{max}$ to rise above the desired 6 bar/degree threshold, which is not favorable but acceptable for the short period where threshold is only exceeded by ≈2.5 bar/deg for one cycle. Such pressure rise rate excursions are difficult to avoid in SI-HCCI transitions near the upper HCCI load limit where fuel quantity is high. The early θ_{50} on the first few HCCI cycles also causes a torque reduction, which is minimal in the high load case but larger in the low load case, most likely because θ_{50} is advanced to a greater extent in the low load case. The maximum NMEP reduction in the low load case occurs over the first two HCCI cycles and reaches ≈0.2 bar = 11% for cylinder $H1$ and ≈0.3 bar = 17% for cylinder $H2$. It can be seen that in terms of absolute values, the maximum reduction is not much worse than other cases; however, because of the lower load reference, the disturbance is larger on a percentage basis. After the first two HCCI cycles, the NMEP is increased to within ≈8% of the reference value; however, it takes several more cycles to converge to the reference. While this amount of error in the torque response may still be passable for drivability, it can be said that it is the least desirable of all cases examined.

One obvious potential reason for the weaker torque tracking at low load is higher error in the HCCI torque model at the low load operating condition. The gradual increase of m_f after the start of the HCCI phase in Fig. 10 supports this hypothesis, as it signals that the IMC output feedback is increasing m_f to compensate for model error. While the output feedback is able to attenuate the model error after several cycles, higher model accuracy would be preferable to minimize the chance of the error occurring. An online adaptation scheme, which aids in attenuating such model error, will be developed later [22]. Another, more subtle possible reason is that the EVC timing at the SI-HCCI switch point θ_{evc}^{swch} was tuned too early for the low load condition, which caused θ_{50} to advance even earlier on the first few HCCI cycles than in other cases.

Summary statistics for the mean and maximum cylinder averaged absolute errors in the SI-HCCI transition performance variables for all tested conditions are given in Table 6. Also listed is the duration of the SI phase of the transition, which can have a significant impact on fuel economy as it limits the amount of time that an engine can be operated in HCCI when the opportunity arises [24]. The duration was found to be ultimately limited by the valve timing set point θ_{evc}^{swch} for the SI phase due to the limitations of the cam phaser actuator dynamics. As load increases, θ_{evc}^{swch} generally retards to reduce the trapped residual mass due to the higher residual temperatures. The controller consequently requires fewer cycles to shift from the nominal SI EVC set point to θ_{evc}^{swch}, which explains why the duration of the SI phase tends to decrease with increasing load. Statistics for the HCCI mode are calculated over five cycles after HCCI entry, since in all conditions only minor transients from the mode transition remained after this point.

To convey the effort involved in calibrating the SI-HCCI transition controller to function across the operating conditions in Figs. 9 and 10, the tuning variables that were varied by operating condition in these experiments are listed below. The values are given in order of increasing load, where the mid load case comes from Fig. 9 and the low and high load cases come from Fig. 10:

- $\theta_{evc}^{swch} = [-40 \quad -23 \quad -14]$ aTDC GE
- $N_{pre}^{evc} = [2 \quad 2 \quad 3]$
- $\lambda^{PS} = [1 \quad 1.05 \quad 1.05]$
- $\theta_{50,f}^{0} = [-9 \quad -6 \quad -3]$ aTDC
- $\theta_{evc}^{*} = [-101 \quad -89 \quad -79]$ aTDC GE
- $\theta_{50,H}^{*} = [3 \quad 5 \quad 7]$ aTDC

All other tuning variables remained constant. As previously stated, it is reasonable to assume that the θ_{evc}^{*} and $\theta_{50,H}^{*}$ set points can be taken from the baseline engine calibration, in which case there are four variables that are tuned by operating condition. Of

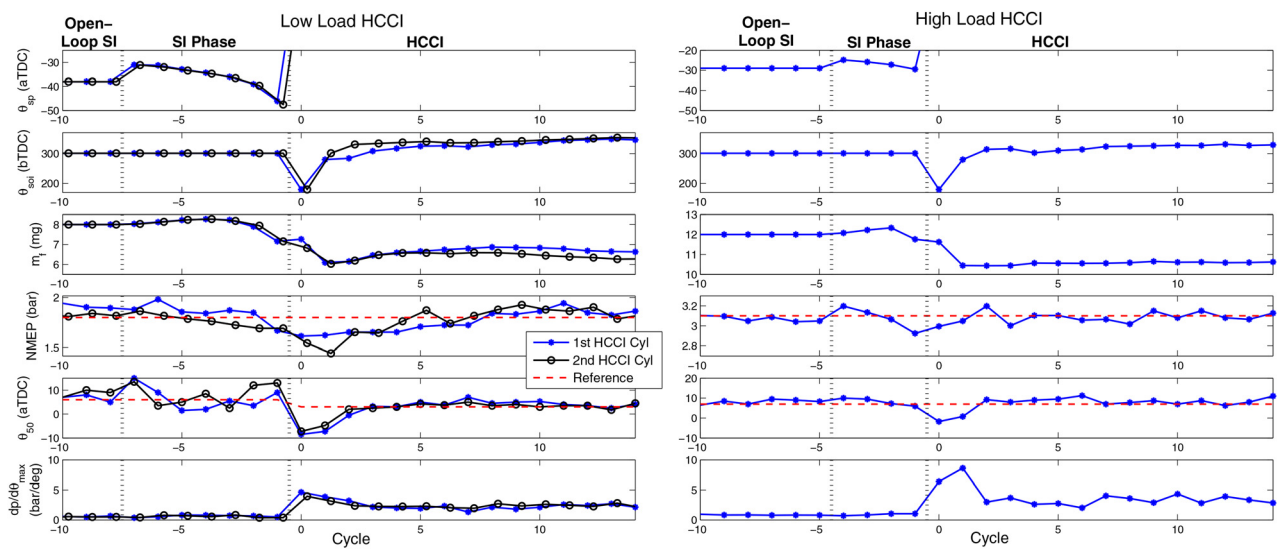

Fig. 10 Controlled SI-HCCI transition experimental results across the HCCI load regime at 2000 rpm. Left: Low load of 1.8 bar NMEP Right: High load of 3.1 bar NMEP. The first and second cylinders to enter HCCI are referred to as *H*1 and *H*2, respectively.

Table 6 Summary of SI-HCCI transition control results

	SI					HCCI					
	$\lvert NMEP - NMEP^* \rvert$ (bar)		$\lvert \theta_{50} - \theta_{50}^* \rvert$ (CAD)			$\lvert NMEP - NMEP^* \rvert$ (bar)		$\lvert \theta_{50} - \theta_{50}^* \rvert$ (CAD)		$dp/d\theta_{max}$ (bar/CAD)	
Load	Mean	Max	Mean	Max	Duration (cycles)	Mean	Max	Mean	Max	Mean	Max
1.8 bar	0.074	0.120	3.50	4.25	7	0.160	0.268	4.02	10.88	2.84	4.27
2.4 bar	0.047	0.089	4.83	11.88	6	0.077	0.138	4.79	9.87	4.09	5.2
3.1 bar	0.0859	0.177	3.12	8.75	4	0.060	0.106	2.80	6.25	4.51	8.62

these four variables, θ_{evc}^{swch} is the main factor influencing the smoothness of the transition, while the other three variables are tuned only with minor tweaks for small performance gains from one operating condition to the next. The controller thus extends across the HCCI load range at 2000 rpm on the experimental engine with variation of only one major parameter and slight adjustments to three minor parameters. The variation in controller tuning with engine speed was not addressed here, but engine speed perturbations will be considered in later experiments [22].

6 Conclusion

A model-based feedback control architecture for reduced calibration and improved generality in SI-HCCI mode transitions has been presented. The control architecture is designed for cam switching SI-HCCI transition strategies, having a structure that provides set points and control elements that inherently implement this type of strategy. The fundamental idea behind the control design is to compensate for disturbances to the engine torque, combustion phasing, and AFR throughout the transition from SI to HCCI using linear feedback throttle control and nonlinear model inverse-based control of fuel injection quantity and timing as well as spark timing. An observer is included in HCCI mode to provide estimates of in-cylinder thermal and compositional states necessary to capture cycle to cycle couplings, and IMC output feedback is included to correct for model errors.

The controller was shown in experiment to carry out SI-HCCI mode transitions across the HCCI load range at 2000 rpm while requiring only one major set point and three minor set points to be adjusted with operating condition. These results compare favorably with previous control designs that incorporated model-based elements, which included open-loop scheduling of actuator sequences by operating condition for all inputs [12], for inputs other than injection timing [15], and for inputs other than throttle and fuel quantity including an intake manifold pressure reference trajectory [13,14]. The range of tested conditions is also comparable or larger than in many previous SI-HCCI mode transition studies, where Refs. [2], [3], [9], [10], and [12] focus on a single load/speed condition, Refs. [7] and [8] test several loads at a single speed, Refs. [11] and [15] test several loads over a 500–650 rpm speed range, and Refs. [13] and [14] contain no experimental results. Additional experiments in Ref. [22], which test the SI-HCCI transition controller over a 500 rpm speed region, make the range of conditions compare even more favorably. The results thus suggest a notable improvement in SI-HCCI transition controller generality and calibration simplicity, which is also tailored for cam switching strategies with two-stage cam mechanisms, which have previously been addressed only with open-loop methods. In Ref. [22], an adaptive parameterization scheme for the combustion model parameters will be developed in order to use online measurements to improve predictive control performance, and several additional SI-HCCI transition experiments will be presented.

Acknowledgment

This material is based upon work supported by the Department of Energy (National Energy Technology Laboratory) under Award No. DE-EE0003533. This work is performed as a part of the ACCESS Project consortium (Robert Bosch LLC, AVL Inc., Emitec Inc., Stanford University, University of Michigan) under the direction of PI Hakan Yilmaz and Co-PI Oliver Miersch-Wiemers, Robert Bosch LLC.

This report was prepared as an account of work sponsored by an agency of the U.S. Government. Neither the U.S. Government nor any agency thereof, nor any of their employees, makes any warranty, express or implied, or assumes any legal liability or responsibility for the accuracy, completeness, or usefulness of any information, apparatus, product, or process disclosed, or represents that its use would not infringe privately owned rights. Reference herein to any specific commercial product, process, or service by trade name, trademark, manufacturer, or otherwise does not necessarily constitute or imply its endorsement, recommendation, or favoring by the U.S. Government or any agency thereof. The views and opinions of authors expressed herein do not necessarily state or reflect those of the U.S. Government or any agency thereof.

Appendix: Controller Equations

Spark Ignition Phase Controller Equations. *Reference p_{im}.* The reference p_{im}^* is derived starting from the SI combustion model's gross cycle work expression, which comes from the work of polytropic compression and expansion processes

$$W_{cig} = \frac{p_{bc}V_{cmb} - p_{ivc}V_{ivc}}{1 - n_c} + \frac{p_{evo}V_{evo} - p_{ac}V_{cmb}}{1 - n_e} \tag{A1}$$

where W_{cig} is the gross cycle work; p_{ivc}, p_{bc}, p_{ac}, p_{evo} are the pressures at IVC/before instantaneous combustion/after instantaneous combustion/EVO; V_{ivc}, V_{cmb}, V_{evo} are the volumes at IVC/instantaneous combustion/EVO; and n represents a polytropic exponent. Volumes are evaluated with the crank slider equation [25], and $V_{cmb} = V(|\theta_{50} - \theta_{50}^{MBT}|)$ following the method of [26].

From polytropic compression

$$p_{bc} = p_{ivc}\left(\frac{V_{ivc}}{V_{cmb}}\right)^{n_c} := b_1 p_{ivc} \tag{A2}$$

$$p_{evo} = p_{ac}\left(\frac{V_{cmb}}{V_{evo}}\right)^{n_e} := b_2 p_{ac} \tag{A3}$$

Equation (A1) can be written as

$$W_{cig} = p_{ivc}\frac{b_1 V_{cmb} - V_{ivc}}{1 - n_c} + p_{ac}\frac{b_2 V_{evo} - V_{cmb}}{1 - n_e} \tag{A4}$$

$$:= c_1 p_{ivc} + c_2 p_{ac} \tag{A5}$$

From constant volume combustion

$$p_{ac} = p_{bc}\left(\frac{T_{ac}}{T_{bc}}\right) = b_1 p_{ivc}\left(\frac{T_{bc} + \Delta T_{cmb}}{T_{bc}}\right) \tag{A6}$$

The expressions for constant volume heat addition, ideal gas law, and polytropic compression give

$$\Delta T_{\text{cmb}} = \frac{m_f Q_{\text{lhv}}}{c_v m_c} \tag{A7}$$

$$m_c = \frac{p_{\text{ivc}} V_{\text{ivc}}}{R T_{\text{ivc}}} \tag{A8}$$

$$T_{\text{bc}} = T_{\text{ivc}} \left(\frac{V_{\text{ivc}}}{V_{\text{cmb}}} \right)^{n_c - 1} \tag{A9}$$

where Q_{lhv} is the fuel lower heating value, c_v is the (fixed) constant volume specific heat, and R is the ideal gas constant. Substituting into Eq. (A6), the expression reduces to

$$p_{\text{ac}} = b_1 p_{\text{ivc}} + \frac{m_f Q_{\text{lhv}} R}{c_v V_{\text{cmb}}} := b_1 p_{ivc} + c_3 \tag{A10}$$

Substituting back into Eq. (A5)

$$W_{\text{cig}} = c_1 p_{\text{ivc}} + c_2 (c_1 p_{\text{ivc}} + c_3) \tag{A11}$$

Now write

$$W_{\text{cig}} = (\text{IMEP}) V_d = (\text{NMEP} - \text{PMEP}) V_d \tag{A12}$$

$$= (\text{NMEP} - (p_{\text{im}} - p_{\text{em}})) V_d \tag{A13}$$

where PMEP denotes pumping mean effective pressure, and

$$m_f = \frac{m_a}{\lambda \text{AFR}_s} = \frac{W_{\text{cyl}}}{\lambda \text{AFR}_s} \frac{120}{N_{\text{eng}} N_{\text{cyl}}} := \frac{1}{c_4} W_{\text{cyl}} \tag{A14}$$

where m_a is the inducted air mass, $N_{\text{cyl}} \equiv 4$ is the number of cylinders, and W_{cyl} is the air flow rate, regressed with $W_{\text{cyl}} = \alpha_1(\theta_{\text{evc}}) p_{\text{im}} + \alpha_0(\theta_{\text{evc}})$ where (θ_{evc}) indicates a functional dependence on θ_{evc}. Applying the constraint equations $\text{NMEP} \equiv \text{NMEP}^*$, $\lambda \equiv \lambda^* \approx 1$, $\theta_{50} = \theta^*_{50,S}$ in Eqs. (A13), (A14), and $V_{\text{cmb}} = V(|\theta_{50} - \theta_{50}^{\text{MBT}}|)$, respectively, and substituting back into Eq. (A11) with $p_{\text{ivc}} = p_{\text{im}}$, p_{im} can be isolated, giving the reference p^*_{im}. The result is

$$p^*_{\text{im}} = \frac{(\text{NMEP}^* + p_{\text{em}}) V_d - c_2 c_3 \alpha_0 / c_4}{c_1 + c_2 b_1 + c_2 c_3 \alpha_1 / c_4 + V_d} \tag{A15}$$

Note that p_{em} is approximated $\approx$1 bar.

Fuel → NMEP. The derivation of m_f^τ, the fuel mass to match the desired torque at MBT combustion phasing, is carried out in the same way as the reference p^*_{im}, except that now the constraint equations change to $\text{NMEP} = \text{NMEP}^*$, $\theta_{50} = \theta^*_{50,S}$, and $p_{\text{im}} = p^y_{\text{im}}$, where p^y_{im} denotes the measured intake manifold pressure, and Eq. (A14) is omitted. Substituting for c_3 from Eq. (A10) into Eq. (A11) allows m_f to be isolated

$$W_{\text{cig}} = c_1 p_{ivc} + c_2 \left(c_1 p_{\text{ivc}} + \frac{m_f Q_{\text{lhv}} R}{c_v V_{\text{cmb}}} \right) \tag{A16}$$

Substituting the definitions of c_1, c_2 from Eq. (A5) with θ_{50} set equal to $\theta^*_{50,S}$ in V_{cmb} into Eq. (A16) along with Eq. (A13) with $\text{NMEP} = \text{NMEP}^*$, and finally setting $p_{\text{ivc}} = p^y_{\text{im}}$, the result for m_f^τ is

$$m_f^\tau = \frac{c_v V_{\text{cmb}}(\theta^*_{50,S})}{Q_{\text{lhv}} R} \left((\text{NMEP}^* - (p^y_{\text{im}} - p_{\text{em}})) V_d - p^y_{\text{im}} c_1 (1 + c_2) \right) \tag{A17}$$

Spark → θ_{50}. The spark timing to θ_{50} expression comes from a direct inversion of the SI combustion model θ_{50} regression. The regression takes the form

$$\theta_{50} = a_1 m_f + a_2 \theta_{\text{sp}}^2 + a_3 \theta_{\text{sp}} + a_4 {\theta_{\text{evc}}}^2 + a_5 \theta_{\text{evc}} + a_6 \lambda'^2 + a_7 \lambda' + a_8 \tag{A18}$$

where a_i are fitting coefficients and $\lambda' = 1/\phi' = (m_a + m_r)/(\text{AFR}_s m_f)$ characterizes the total dilution in the cylinder. m_a and m_r are evaluated using the current θ_{evc} and p_{im} measurements, and m_f is taken as the output of the fuel controller which executes before the spark timing controller. Setting

$$\beta_2 = a_2 \tag{A19}$$

$$\beta_1 = a_3 \tag{A20}$$

$$\beta_0 = a_1 m_f + a_4 \theta_{\text{evc}}^2 + a_5 \theta_{\text{evc}} + a_6 \lambda'^2 + a_7 \lambda' + a_8 - \theta^*_{50} \tag{A21}$$

Equation (A18) can be solved for θ_{sp} using the quadratic equation. The maximum root (in units of aTDC) is chosen as the correct root because inspection shows that the minimum root occurs unreasonably early spark timings after the quadratic dependence on θ_{sp} shifts inflection.

Homogeneous Charge Compression Ignition Phase Controller Equations. *Fuel → NMEP*. The HCCI combustion model m_f to NMEP inversion follows the same logic for that of the SI combustion model; the equation for the gross cycle work is given by Eq. (A1), and the constraint equations $\text{NMEP} = \text{NMEP}^*$, $\theta_{50} = \theta^*_{50,S}$, and $p_{\text{im}} = p^y_{\text{im}}$ are imposed. The main difference in solving for m_f is caused by the appearance of the combined thermal and combustion efficiency from the HCCI model of Ref. [19], $\eta_\lambda = (a_{\eta 1} \lambda_c + a_{\eta 2})/(\lambda_c + a_{\eta 3})$, so that the equivalent of Eq. (A16) takes the form

$$W_{\text{cig}} = c_1 p_{\text{ivc}} + c_2 \left(c_1 p_{\text{ivc}} + \frac{m_f Q_{\text{lhv}} R}{c_v V_{\text{cmb}}} \frac{a_{\eta 1} \lambda_c + a_{\eta 2}}{\lambda_c + a_{\eta 3}} \right) \tag{A22}$$

where $a_{\eta i}$, $i = 1, 2, 3$ are fitting coefficients and $\lambda_c = (m_a + m ra)/(\text{AFR}_s m_f) = (m_a + m_r(1 - \hat{b}_{\text{bd}} - \hat{f}_{\text{bd}}))/\text{AFR}_s m_f$. Evaluating m_a and m_r with the estimated states and measured quantities and substituting in for λ_c, it can be shown that Eq. (A22) reduces to a quadratic polynomial in m_f with the following coefficients:

$$\beta_2 = a_{\eta 2} \tag{A23}$$

$$\beta_1 = \frac{a_{\eta 1}(m_a + m_r)}{\text{AFR}_s} - \frac{d_2 a_{\eta 3}}{d_1} \tag{A24}$$

$$\beta_0 = -\frac{d_2 (m_a + m_r)}{d_1 \text{AFR}_s} \tag{A25}$$

where

$$d_1 := \frac{Q_{\text{lhv}} R V_{\text{cmb}} (\theta^*_{50})^{n_c - 1}}{c_v p_{\text{ivc}} V_{\text{ivc}}^{n_c}} \tag{A26}$$

$$d_2 := \frac{(\text{NMEP}^* - \text{PMEP}) V_d - c_1 p_{\text{ivc}}}{c_2 b_1 p_{\text{ivc}}} - 1 \tag{A27}$$

and hence can be readily solved for m_f (note $p_{\text{ivc}} = p^y_{\text{im}}$). The maximum root of the quadratic equation is selected, as the minimum root tends to be negative which is not physical.

SOI → θ_{50}. The calculation for θ_{soi} involves inversion of an integrated Arrhenius rate expression with a parameterized threshold K_{th} that comes from Ref. [19] with a simplified recompression temperature dependence

$$K_{\text{th}}(\theta_{\text{soi}}, \lambda_r, T_{\text{rc}}) = \int_{\theta_{\text{ivc}}}^{\theta_{\text{soc}}} \frac{1}{\omega} p_c(\theta)^{n_p} e^{\left(\frac{-E_a}{RT_c(\theta)}\right)} d\theta \tag{A28}$$

$$K_{\text{th}}(\theta_{\text{soi}}, \lambda_r, T_{rc}) = (a_{12}\lambda_r^2 + a_{11}\lambda_r + a_{10})\theta_{\text{soi}} + a_{02}\lambda_r^2 + a_{01}\lambda_r + a_{00} + a_T T_{\text{rc}} \tag{A29}$$

$$p_c(\theta) = p_{\text{ivc}}\left(\frac{V_{ivc}}{V(\theta)}\right)^{n_c},\ T_c(\theta) = T_{\text{ivc}}\left(\frac{V_{\text{ivc}}}{V(\theta)}\right)^{n_c-1} \tag{A30}$$

where λ_r is the recompression relative AFR and T_{rc} is the recompression temperature. The inversion is carried out by finding the value of the threshold K_{th} which gives the desired start of combustion timing θ^*_{soc}, which is backsolved from the linear fit from θ_{50} to θ_{soc}, $\theta^*_{\text{soc}} = (\theta_{50} - a_{\text{soc},0})/a_{\text{soc},1}$. The integral is evaluated up to θ^*_{soc} using the estimated T_{ivc} and p_{ivc} in Eq. (A30) to get the desired threshold

$$K^*_{\text{th}} = \int_{\theta_{\text{ivc}}}^{\theta^*_{\text{soc}}} \frac{1}{\omega} p_c(\theta)^{n_p} e^{\left(\frac{-E_a}{RT_c(\theta)}\right)} d\theta \tag{A31}$$

Setting $K_{\text{th}} = K^*_{\text{th}}$ and solving for θ_{soi} gives

$$\theta_{\text{soi}} = \frac{K^*_{\text{th}} - a_{02}\lambda_r^2 - a_{01}\lambda_r - a_{00} - a_T T_{\text{rc}}}{a_{12}\lambda_r^2 + a_{11}\lambda_r + a_{10}} \tag{A32}$$

Note that the evaluation of K^*_{th} in Eq. (A31) requires iteration and is thus computationally intensive. To facilitate real-time implementation, p_{ivc} and ω are factored out of the Arrhenius integral to give

$$\frac{K^*_{\text{th}}\omega}{p^{n_p}_{\text{ivc}}} = \int_{\theta_{\text{ivc}}}^{\theta^*_{\text{soc}}} \left(\frac{V_{\text{ivc}}}{V(\theta)}\right)^{n_c n_p} e^{\left(\frac{-E_a}{RT_c(\theta)}\right)} d\theta \tag{A33}$$

The right-hand side of this equation can be solved as a function of T_{ivc} and θ^*_{soc} (neglecting the impact of IVC timing) and stored in a two-dimensional look-up table. The term $K^*_{\text{th}}\omega/p^{n_p}_{\text{ivc}}$ can then be solved for K^*_{th}, hence bypassing the iterative calculation in real-time.

References

[1] Zhao, F., Asmus, T., Assanis, D., Dec, J., Eng, J., and Najt, P., 2003, *Homogeneous Charge Compression Ignition (HCCI) Engines: Key Research and Development Issues*, SAE International, Warrendale, PA.

[2] Koopmans, L., Ström, H., Lundgren, S., Backlund, O., and Denbratt, I., 2003, "Demonstrating a SI-HCCI-SI Mode Change on a Volvo 5-Cylinder Electronic Valve Control Engine," SAE Technical Paper No. 2003-01-0753.

[3] Santoso, H., Matthews, J., and Cheng, W., 2005, "Managing SI/HCCI Dual-Mode Engine Operation," SAE Technical Paper No. 2005-01-0162.

[4] Zhang, Y., Xie, H., Zhou, N., Chen, T., and Zhao, H., 2007, "Study of SI-HCCI-SI Transition on a Port Fuel Injection Engine Equipped With 4VVAS," SAE Technical Paper No. 2007-01-0199.

[5] Milovanovic, N., Blundell, D., Gedge, S., and Turner, J., 2005, "SI-HCCI-SI Mode Transition at Different Engine Operating Conditions," SAE Technical Paper No. 2005-01-0156.

[6] Tian, G., Wang, Z., Ge, Q., Wang, J., and Shuai, S., 2007, "Control of a Spark Ignition Homogeneous Charge Compression Ignition Mode Transition on a Gasoline Direct Injection Engine," Proc. Inst. Mech. Eng., Part D, **221**(7), pp. 867–875.

[7] Cairns, A., and Blaxill, H., 2007, "The Effects of Two-Stage Cam Profile Switching and External EGR on SI-CAI Combustion Transitions," SAE Technical Paper No. 2007-01-0187.

[8] Kalian, N., Zhao, H., and Qiao, J., 2008, "Investigation of Transition Between Spark Ignition and Controlled Auto-Ignition Combustion in a v6 Direct-Injection Engine With Cam Profile Switching," Proc. Inst. Mech. Eng., Part D, **222**(10), pp. 1911–1926.

[9] Wu, H., Collings, N., Regitz, S., Etheridge, J., and Kraft, M., 2010, "Experimental Investigation of a Control Method for SI-HCCI-SI Transition in a Multi-Cylinder Gasoline Engine," SAE Technical Paper No. 2010-01-1245.

[10] Nier, T., Kulzer, A., and Karrelmeyer, R., 2012, "Analysis of the Combustion Mode Switch Between SI and Gasoline HCCI," SAE Technical Paper No. 2012-01-1105.

[11] Kakuya, H., Yamaoka, S., Kumano, K., and Sato, S., 2008, "Investigation of a SI-HCCI Combustion Switching Control Method in a Multi-Cylinder Gasoline Engine," SAE Technical Paper No. 2008-01-0792.

[12] Widd, A., Johansson, R., Borgqvist, P., Tunestål, P., and Johansson, B., 2011, "Investigating Mode Switch From SI to HCCI Using Early Intake Valve Closing and Negative Valve Overlap," SAE Technical Paper No. 2011-01-1775.

[13] Yang, X., and Zhu, G., 2013, "SI and HCCI Combustion Mode Transition Control of an HCCI Capable SI Engine," IEEE Trans. Control Syst. Technol., **21**(5), pp. 1558–1569.

[14] Zhang, S., and Zhu, G., 2014, "Model-Based Mode Transition Control Between SI and HCCI Combustion," ASME Paper No. DSCC2014-6148.

[15] Ravi, N., Jagsch, M., Oudart, J., Chaturvedi, N., Cook, D., and Kojic, A., 2013, "Closed-Loop Control of SI-HCCI Mode Switch Using Fuel Injection Timing," ASME Paper No. DSCC2013-3785.

[16] Gorzelic, P., 2015, "Modeling and Model-Based Control of Multi-Mode Combustion Engines for Closed-Loop SI/HCCI Mode Transitions with Cam Switching Strategies," Ph.D. thesis, The University of Michigan, Ann Arbor, MI.

[17] Song, H. H., and Edwards, C. F., 2009, "Understanding Chemical Effects in Low-Load-Limit Extension of Homogeneous Charge Compression Ignition Engines Via Recompression Reaction," Int. J. Eng. Res., **10**(4), pp. 231–250.

[18] Nüesch, S., Stefanopoulou, A., Jiang, L., and Sterniak, J., 2014, "Fuel Economy of a Multimode Combustion Engine With Three-Way Catalytic Converter," ASME J. Dyn. Syst., Meas., Control, **137**(5), p. 051007.

[19] Gorzelic, P., Shingne, P., Martz, J., Stefanopouou, A., Sterniak, J., and Jiang, L., 2016, "A Low-Order Adaptive Engine Model for SI-HCCI Mode Transition Control Applications With Cam Switching Strategies," Int. J. Eng. Res., **17**(4), pp. 451–468.

[20] Eriksson, L., 2007, "Modeling and Control of Turbocharged SI and DI Engines," Oil Gas Sci. Technol.-Rev. IFP, **62**(4), pp. 523–538.

[21] Gorzelic, P., Hellström, E., Stefanopoulou, A., and Jiang, L., 2012, "Model-Based Feedback Control for an Automated Transfer Out of SI Operating During SI to HCCI Transitions in Gasoline Engines," ASME Paper No. DSCC2012-MOVIC2012-8779.

[22] Gorzelic, P., Sterniak, J., and Stefanopoulou, A., 2017, "SI-HCCI Mode Transitions Without Open-Loop Sequence Scheduling: Online Parameter Adaptation," ASME J. Dyn. Sys., Meas., Control, (accepted).

[23] Schwarzmann, D., 2007, "Nonlinear Internal Model Control with Automotive Applications," Ph.D. thesis, Ruhr-Universität Bochum, Bochum, Germany.

[24] Nüesch, S., Gorzelic, P., Jiang, L., Sterniak, J., and Stefanopoulou, A., 2016, "Accounting for Combustion Mode Switch Dynamics and Fuel Penalties in Drive Cycle Fuel Economy," Int. J. Eng. Res., **17**(4), pp. 436–450.

[25] Heywood, J., 1992, *Internal Combustion Engine Fundamentals*, McGraw-Hill, New York.

[26] Eriksson, L., and Andersson, I., 2002, "An Analytic Model for Cylinder Pressure in a Four Stroke SI Engine," SAE Technical Paper No. 2002-01-0371.